

Glass transition and layering effects in confined water: A computer simulation study

P. Gallo^{a)} and M. Rovere

Dipartimento di Fisica, Università "Roma Tre," Istituto Nazionale per la Fisica della Materia, Unità di Ricerca Roma Tre, Via della Vasca Navale 84, 00146 Roma, Italy

E. Spohr

Department of Theoretical Chemistry, University of Ulm, Albert-Einstein-Allee 11, D-89069 Ulm, Germany

(Received 29 June 2000; accepted 2 October 2000)

Single particle dynamics of water confined in a nanopore is studied through computer molecular dynamics. The pore is modeled to represent the average properties of a pore of Vycor glass. Dynamics is analyzed at different hydration levels and upon supercooling. At all hydration levels and all temperatures investigated a layering effect is observed due to the strong hydrophilicity of the substrate. The time density correlators show, already at ambient temperature, strong deviations from the Debye and the stretched exponential behavior. Both on decreasing hydration level and upon supercooling we find features that can be related to the cage effect typical of a supercooled liquid undergoing a kinetic glass transition. Nonetheless the behavior predicted by mode coupling theory can be observed only by carrying out a proper shell analysis of the density correlators. Water molecules within the first two layers from the substrate are in a glassy state already at ambient temperature (bound water). The remaining subset of molecules (free water) undergoes a kinetic glass transition; the relaxation of the density correlators agree with the main predictions of the theory. From our data we can predict the temperature of structural arrest of free water. © 2000 American Institute of Physics. [S0021-9606(00)52248-X]

I. INTRODUCTION

The modification of the dynamical properties of liquids in a confined environment relative to the bulk is a field of rapidly growing interest because of the close connection with relevant technological and biophysical problems. The specific differences in behavior are, among others, due to different interactions between liquid and substrate, the size of the confining region, and the size of the particles composing the liquid. Nonetheless some underlying common features can be sorted out of the extremely rich and diversified phenomenology available.¹ In fact there are two main causes for the change of dynamics of a confined liquid with respect to its bulk phase: the first is the influence of the interactions of the liquid with a rough surface, which is expected to slow down the dynamics; the second is the confinement effect that can lead to an increase in the free volume of a molecule, which then results in accelerated dynamics together with a decrease of the glass transition temperature relative to the one of the bulk phase. The interplay between these two effects depends crucially on the particle density and the size of the confining system.²⁻⁵

In particular, the dynamical properties of water in restricted geometries and at interfaces have recently been studied intensely because of the important effects in systems of interest to biology, chemistry, and geophysics, whose behavior depends on how the pore size and structure influence the diffusion of water. Those properties are particularly relevant

in understanding phenomena like the mobility of water in biological channels^{6,7} or the dynamics of hydrated proteins.⁸

It is well known that liquid water shows a very peculiar behavior in the supercooled phase. The study of water approaching a glass phase is still a challenging problem since below 235 K one enters the so-called *no man's land*,⁹ where nucleation processes take place and drive the liquid to the solid crystalline phase, preventing the observation of the glass transition.^{10,11} It is unclear until now how confinement could change this scenario. It would be particularly important to understand whether the glass transition temperature could be experimentally accessible for confined water. In this respect the modifications induced by the confinement on the dynamics of water on supercooling are of extreme interest.

Computer simulation is a very suitable tool for exploring the liquid in the range of the supercooled regime without the limitations of the nucleation process which takes place in the real experiment. Dynamical properties of different types of liquids in confined geometries have been studied in recent years by computer simulation.^{5,12-14} For water confined in micropores there are a number of computer simulation studies on the mobility of water.^{6,7,15,16} It is still difficult, however, to find general trends; systematic studies of the dynamics of confined water have not been attempted until now.

For confined and interfacial water, inelastic neutron scattering and nuclear magnetic resonance (NMR) spectroscopy found a slowing down of the dynamics relative to the bulk phase.¹⁷⁻²¹ For water in contact with proteins there are also signatures of a transition of adsorbed water to a glassy state, which is driven by the protein surface.⁸ Moreover, recent

^{a)}Author to whom correspondence should be addressed. Electronic mail: gallop@fis.uniroma3.it

simulation and experimental studies showed a typical spectral glassy anomaly, the so-called boson peak.^{22,23}

In the many experimental studies of confined water that have been performed, water in Vycor is of particular interest,¹⁷ since Vycor is a porous silica glass characterized by a quite sharp distribution of pore sizes with an average diameter of 40 Å. The pore size does not depend on the hydration level and the surface of the pore is strongly hydrophilic. Moreover, the water-in-Vycor system can be considered as a prototype for more complex situations of interfacial water.^{24,25}

In this article we present the results of a molecular dynamics study of the single-particle dynamics of water confined in a silica cavity modeled to represent the average properties of the pores of Vycor glass.^{26,27} We will concentrate on the dynamical behavior of the confined water at half-hydration on supercooling. In previous studies, the static properties of this system were investigated.^{26,27}

In the second section we recall the general theoretical background which concerns the modern interpretation of the glass transition and we will concentrate on a short description of the mode coupling theory (MCT).²⁸ In Sec. III we explain the technical details of our simulation of molecular dynamics (MD). In Sec. IV we discuss the important layering effect that we observe in the confined water. This effect forms the basis for a layer analysis of the dynamical results that we introduced for the density correlator.²⁹ In Sec. V this analysis is carried out for the system at ambient conditions. By means of this layer analysis we can find agreement with the MCT predictions and estimate the values of some relevant parameters of the theory as exposed in Sec. VI where the properties of the system upon supercooling are analyzed. Section VII is devoted to the conclusions of our work.

II. THE PHYSICS OF THE GLASS TRANSITION

A. The glass transition scenario

Glasses are a very popular subject of the contemporary science literature. However, in spite of the huge experimental, computational, and theoretical efforts made, a unified picture able to account for the behavior of the liquid from its normal state throughout supercooling and vitrification is still lacking. Theoretical physicists are developing a first principle theory for glasses,^{30,31} based on the phenomenological ideas introduced by Kauzmann³² and developed later by Adam, Gibbs, and Di Marzio.³³

A scenario emerges that can be pictured by considering the free energy landscape or alternatively the potential energy landscape.³⁴ In the high-temperature regime, the free energy functional has only one relevant minimum and correspondingly there are several directions in the configurational space with negative eigenvalues. The liquid behaves “normally,” and diffusion is stochastic, i.e., there is only one relevant time scale and the relaxation process is of Debye type. As one starts supercooling (i.e., cooling the system below the melting temperature T_m) the system approaches an important crossover temperature T_C referred to as the temperature of kinetic glass transition. MCT²⁸ in its idealized version is able to describe the dynamics of the liquid in great

detail with precise predictions on the behavior and the analytical shape of the density correlators (see next subsection) for systems sufficiently close to, yet above, T_C . The region above T_C is only landscape influenced.³⁵ At $T=T_C$ the number of directions leading to different basins goes to zero.^{36–38} In the region below T_C there is an exponentially large number of minima in the free energy separated by barriers that are high compared to thermal energy. In this respect T_C represents a cross-over temperature from a liquidlike regime to a solidlike regime where only hopping processes can restore ergodicity. Below T_C the supercooled liquid is, in fact, frequently trapped in one of the local free energy minima and only activated processes take the system from one minimum to another one in the energy landscape.³³ This region is strongly landscape dominated.³⁵

In the “many valley picture” the liquid–glass transition occurs at the Kauzmann temperature T_K , where the configurational entropy, which measures the logarithm of the number of accessible minima, vanishes and, correspondingly, the free energy barriers diverge.^{30,31,39,40} The transition at T_K can be considered as an ideal glass transition which can take place only at an infinitely slow cooling rate, where it would be signaled by the divergence of the viscosity. This ideal second-order transition is related to the singularities which are found at finite cooling rate in experiments at the conventional glass transition temperature, T_g , where $T_K < T_g < T_C$.

B. Predictions of the mode coupling theory

In this article we will focus on the relatively high-temperature region where dynamics can be studied by MD, i.e., the supercooled region where T is above and approaches T_C . Here MCT in its idealized version works very well for many systems.⁴¹

MCT is able to describe the dynamics of a liquid when the single entity, molecule or atom, is trapped by the transient cage formed by its nearest neighbors. This transient caging is responsible for the stretching of the relaxation laws and the separation of time scales. In its idealized version MCT does not take into account the hopping processes. This version predicts a transition to a nonergodic system at T_C , when all the cages are frozen. Nonetheless, hopping processes are not relevant for most liquids above T_C . An asymptotic expansion in the region near the ideal singularity (at T_C) yields predictions of the functional form of the time correlators and the critical exponents. These predictions have been tested both by experiments and MD simulations for many glass formers. MCT thus renders possible, among others, an estimate of the behavior of the time correlators close to the crossover temperature.^{28,41}

MCT predicts a two-step relaxation for the dynamics, which is the signature of the cage effect. Well above T_C , after an initial ballistic regime, the particle enters the stochastic diffusion regime, and its mean square displacement (MSD) increases linearly with time. In the supercooled region above T_C , after the short time ballistic regime, the particle is trapped by the barrier created by the nearest-neighbor cage; Brownian diffusion is restored only when this cage relaxes. This behavior is reflected in the self part of the den-

sity autocorrelation function, and in any other correlator which has a nonzero overlap with the density. In particular, when approaching T_C from the liquid side, the Fourier transform of the density correlator, the self intermediate scattering function (ISF), $F_S(Q, t)$, has a two-step relaxation behavior with a fast and a slow decay. After the fast decay it enters a plateau region, corresponding to the rattling of the particle in the nearest-neighbor cage, which is called the β -relaxation region. After the time interval of the plateau, which becomes longer when approaching T_C , the function $F_S(Q, t)$ decays to zero. This long time relaxation is called α -relaxation. In the α -relaxation region it has been shown that the relaxation process is well described by a stretched exponential

$$F_S(Q, t \rightarrow \infty) \sim e^{-(t/\tau_l)^\beta}, \quad (1)$$

where τ_l is the long relaxation time and β is called the Kohlrausch exponent. MCT predicts that, when T_C is approached, the α -relaxation takes place on increasingly longer time scales, so that the relaxation time τ_l diverges with a power law

$$\tau_l \sim (T - T_C)^{-\gamma}. \quad (2)$$

As a consequence, the diffusion coefficient D , which is predicted to be proportional to τ_l^{-1} , goes to zero at T_C with the power law $D \sim (T - T_C)^\gamma$.

In the idealized version of MCT the system becomes nonergodic at T_C , defined as the temperature of structural arrest; below T_C the cages are frozen and only hopping processes can restore ergodicity. Extended MCT⁴² takes into account this effect.

Finally, we recall that, since the MCT description of the kinetic glass transition is based on the cage effect, the relevant length scales are of the order of the nearest-neighbor distances. Consequently the dynamical quantities in Q space display this effect most clearly for values of Q close to the maximum of the static structure factor $S(Q)$.

C. Bulk supercooled water and MCT

In recent years it was discovered that simple point charge/extended (SPC/E)⁴³ supercooled water has a temperature of structural arrest T_C (Ref. 44) coinciding with the so-called singular temperature T_s of Speedy and Angell.⁴⁵ As stated above, MCT predicts that close to T_C the liquid dynamics is dominated by the ‘‘cage effect.’’ Water does not behave like normal glass-forming fluids in this regard, since the cage effect is not a consequence of an increase of density upon supercooling but, rather, seems to be determined by the increase of the hydrogen bond stiffness, which makes the cage more rigid as the temperature is lowered below room temperature. The long time behavior of the single particle dynamics is well described in terms of the MCT and the dependence of τ_l (and D) on temperature are found to agree with the power law, Eq. (2). Successive simulations over a wide range of pressures and temperatures⁴⁶ and theoretical studies⁴⁷ fully confirmed the MCT behavior of this potential.

III. MOLECULAR DYNAMICS OF WATER IN VYCOR: TECHNICAL DETAILS

Vycor is a porous silica glass obtained by spinodal decomposition of a glass-forming melt of SiO_2 and B_2O_3 . The B_2O_3 -rich phase is leached out, leaving a SiO_2 porous glass. The main differences of Vycor glass with respect to other analogous porous media are that it has a well-characterized structure with a quite sharp distribution of pore sizes and a strong hydrophilic surface. The void fraction, 28%, is an interconnected network of pores of diameter ~ 40 Å. Vycor has a strong capability to absorb water, since its equilibrium hydration at ambient conditions is 25% of its dry weight. Furthermore, its pores do not change size when filled with water. For these reasons it can be considered as a good candidate to study the general behavior of water in hydrophilic nanopores as a function of the level of hydration.²⁴

During experimental sample preparation, after the desiccation process and before introducing water into the pores, those oxygen atoms on the internal surfaces whose valences are not saturated (called nonbridging oxygens) are saturated with hydrogen atoms.

In our simulation we build up a cubic cell of silica glass by the usual procedure of melting a β -cristobalite crystalline structure at 6000 K and quenching to room temperature. As described in details in previous work^{26,27} we get a cube of length $L = 71.29$ Å. Inside the cube we carve a cylindrical cavity of 40 Å diameter by eliminating all the atoms lying within a distance $R = 20$ Å from the axis of the cylinder taken as the z axis. Then we exclude all the silicons with less than four oxygen neighbors. On the surface of the pore we distinguish the oxygen atoms which are bonded to two silicons [so-called bridging oxygens (BO)] from those which are bonded to only one silicon atom called nonbridging oxygens (NBO). The NBOs are saturated with hydrogen atoms. The final block of material contains 6155 silicon atoms, 12 478 BOs, and 227 NBOs saturated by 227 acidic hydrogens (AHs). The surface density of AHs is 2.5 nm^{-2} , in good agreement with the experimentally determined value of 2.3 nm^{-2} .⁴⁸

Water molecules described by the simple point charge/extended (SPC/E) model⁴³ are introduced in the cavity. The SPC/E potential is one of the most frequently used interaction site models for water. Both density and diffusion coefficient show remarkably good agreement with experiment at ambient condition.⁴³ It has to be stressed that SPC/E exhibits a minimum in the pressure P vs T at about 240 K, while the experimental temperature of maximum density is located at $T \approx 277$ K. We therefore expect the phase diagram of SPC/E water to be shifted downwards in temperature relative to the experimental one.^{49,50}

The water sites interact with the atoms of the rigid matrix by means of an empirical potential model,^{26,51} where different fractional charges are assigned to the sites of the silica glass. In addition, the oxygen sites of water interact with BOs and NBOs of the substrate via Lennard-Jones potentials. All parameters are collected in Table I.

The molecular dynamics is performed in the microcanonical ensemble with a time step of 2.5 fs. Each run was equilibrated via a coupling to a temperature ‘‘reservoir’’ by

TABLE I. Parameters of the SPC/E model and of the substrate–water interaction potential.

	Site	σ (Å)	ϵ/k_B (K)	q e
Water ^a	O	3.166	78.22	-0.848
	H	0.0	0.0	0.424
Silica ^b	H	0.0	0.0	0.424
	Si	0.0	0.0	1.283
	BO	2.70	230.0	-0.629
	NBO	3.00	230.0	-0.533
	AH	0.0	0.0	0.206

^aSPC/E model (Ref. 43).

^bValues from Ref. 51; BO: bridging oxygens; NBO: nonbridging oxygens; AH: protons on the substrate surface.

using the Berendsen method of velocity rescaling. Data during the initial equilibration period were discarded, until monitored quantities like the internal energy showed no trends with time.

Since the simulations of such a large system are rather time consuming, we used the shifted force method with a cutoff at 9 Å for all interactions. We checked that the use of a larger cutoff or Ewald summations does not change the trend of the obtained results, as discussed in previous work.²⁷ Since we need to store long trajectories for a large number of molecules, we minimized the disk space by saving them at a logarithmic time step. With this choice the size of trajectories for 2000 molecules lasting 1 ns is roughly 1.5 GB. For the lower temperatures several runs of 1 ns each were performed.

In the following we will present data for five hydration levels of the pore at ambient temperature, as described in Table II. For the case of roughly half-hydration, which corresponds to $N_W = 1500$ water molecules, we studied five temperatures, namely $T = 298, 270, 240, 220$ and 210 K.

IV. DENSITY PROFILES OF CONFINED WATER

In the experiments on water confined in Vycor the full hydration is obtained by immersion of the dry sample in water. Vycor glass adsorbs water up to 25% of its dry weight, so the full hydration in the experiment is defined as $h_f \approx 0.25$ g of water/g of Vycor. A partial hydration is experimentally obtained by exposing the fully hydrated sample to P_2O_5 for a number of hours in order to reduce the water content and reach the desired ratio $h = (\text{mass of water})/(\text{mass of Vycor})$.²⁴

TABLE II. Hydration levels of the pore. N_W is the number of water molecules and ρ_W the corresponding global density. The hydration level is based on estimated value for full hydration $N_W \sim 2600$ molecules (see text).

N_W	% hydration	ρ_W (g/cm ²)
500	19%	0.1687
1000	38%	0.3373
1500	56%	0.4971
2000	75%	0.6658
2600	98%	0.8788

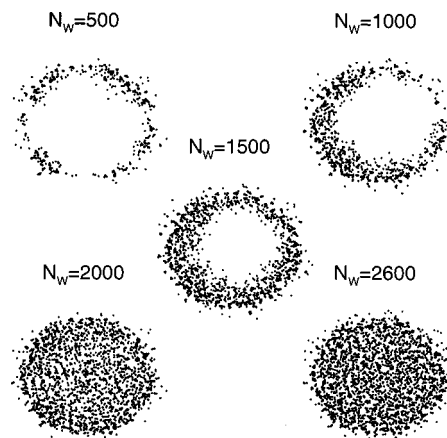


FIG. 1. Snapshots of equilibrium configurations of confined water at different hydration levels (see Table II). Only the oxygen atoms of water are shown projected on the xy plane perpendicular to the axis of the confining cylinder.

The full hydration in the experiment ($h = h_f$) corresponds to a density of water⁵² $\rho_f = 0.8877$ g cm⁻³, which is 11% lower with respect to bulk water. In the computer simulation we vary the hydration level by changing the number of molecules inserted in the single cylindrical cavity of our simulation cell. We assume that the full hydration corresponds to the experimental density ρ_f which would be given in our simulation by a number of water molecules $N_W \approx 2600$. Levels of hydration are given relative to this value.

In Fig. 1 we show snapshots at ambient temperature for the five different hydration levels studied, $N_W = 500$ ($\approx 20\%$), $N_W = 1000$ ($\approx 40\%$), $N_W = 1500$ ($\approx 60\%$), $N_W = 2000$ ($\approx 75\%$), and $N_W = 2600$ ($\approx 100\%$), as in Table II. We observe that the pore is strongly hydrophilic, since molecules bind strongly to the surface even at low levels of hydration.

The lowest hydration level is lower than the monolayer coverage estimated to be 25% of hydration.²¹ In the inner surface of the pore single water molecules or small patches of water molecules are found.

The radial density profiles normalized to the bulk water density are shown in Fig. 2 as a function of $R = \sqrt{x^2 + y^2}$. The formation of well-defined layers of water molecules close to the substrate is evident in the region between 15 and 20 Å, where the pore surface is located. For the highest level of hydration water fills the pore completely. In the pore center a density close to the experimental density at full hydration is reached.

Layering effects of confined water have been observed in almost all computer simulations performed in different geometry and with different water–substrate interaction.¹⁵ In our case they are representative of the high hydrophilicity of the pore. In particular, we note that, as the hydration level is increased, a double layer structure with density oscillations is formed. Another consequence of the hydrophilic interaction is the distortion of the hydrogen bond network of water in the layers close to the substrate.^{26,27} Since the inner surface is corrugated, we do observe that the density is different from zero also right inside the pore surface, where water molecules are trapped in small pockets inside the substrate.

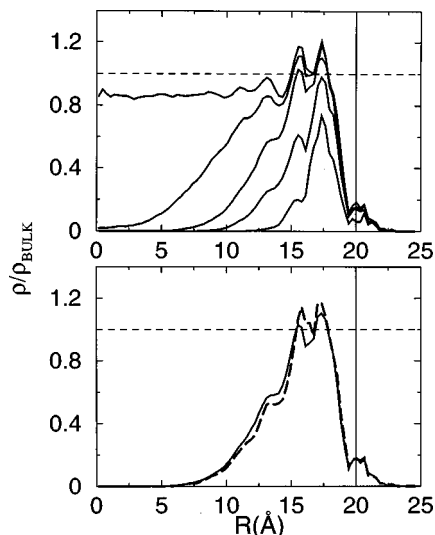


FIG. 2. Density profiles of confined water along the cylindrical radius $R = \sqrt{x^2 + y^2}$ normalized to the bulk water density at ambient temperature. Top: density profiles at $T=298$ for decreasing levels of hydration (from $N_w=2600$ to $N_w=500$ from top to bottom). A small fraction of the water molecules is trapped inside the silica glass, which leads to the density contribution for $R > 20 \text{ \AA}$, where the confining surface is located. Bottom: density profiles for $N_w=1500$ at ambient temperature, $T=298$ K (continuous line), and in the supercooled regime, $T=210$ K (long dashed line).

These molecules do not contribute to the diffusion dynamics of water.

A decrease of temperature has no large effect on the density profiles, as can be seen in the lower part of Fig. 2 where the case $N_w=1500$ is shown at ambient temperature ($T=297$ K) and in the supercooled regime ($T=210$ K). We note that the peak heights of the two layers become more pronounced as the temperature is lowered.

V. SLOW DYNAMICS OF CONFINED WATER: THE ROLE OF HYDRATION AT AMBIENT TEMPERATURE

We will consider now the single-particle translational dynamics of the oxygens of water as a function of hydration level at ambient temperature. In Fig. 3 we display the mean square displacement (MSD) $\langle r^2(t) \rangle = \langle |\mathbf{r}(t) - \mathbf{r}(0)|^2 \rangle$ in three dimensions $\langle r^2 \rangle = \langle x^2 \rangle + \langle y^2 \rangle + \langle z^2 \rangle$ as a function of time for the different hydration levels. The plot is on a log-log scale in order to make more evident the flattening of the curves at lower hydrations. After the initial ballistic regime, where the MSD increases proportional to t^2 (up to $t \approx 0.4$ ps), the curves begin to flatten at intermediate times. This behavior becomes more evident as the hydration level is decreased. While the onset of the cage effect is almost independent of the hydration, the relaxation time of the cage depends strongly on the hydration level. The lowering of the hydration affects the mobility of water already at room temperature by shifting the onset of the diffusive behavior ($\text{MSD} \propto t$) to larger times.^{53,29} In the inset the diffusion coefficient, extracted from the slope of the MSD in the diffusive regime, is plotted as a function of the number of particles inside the pore. The SPC/E bulk water value is also displayed. We note substantial decrease of the mobility of confined water as the hydration level is lowered.

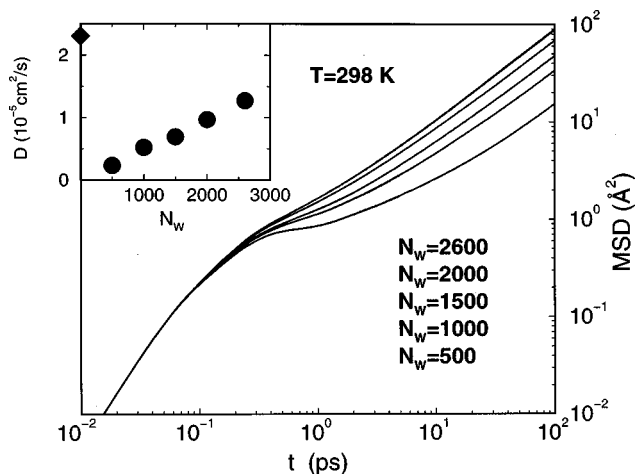


FIG. 3. Mean square deviation (MSD) of the oxygen atoms $\langle r^2(t) \rangle = \langle |\mathbf{r}(t) - \mathbf{r}(0)|^2 \rangle$ for diffusion in three dimensions as a function of time, t , for different levels of hydration from top ($N_w=2600$) to bottom ($N_w=500$). In the inset the diffusion coefficients extracted from the slopes of the MSD curves are displayed as a function of the hydration level (filled circles). For comparison the bulk value for SPC/E water at ambient conditions is also shown (filled diamond).

As can be expected, the different regimes in the diffusion are also reflected in the behavior of the single-particle intermediate scattering function (ISF), $F_S(Q, t)$. This is the Fourier transform of the Van Hove self-correlation function

$$G_S(r, t) = \frac{1}{N} \left\langle \sum_{i=1}^N \delta[\mathbf{r} + \mathbf{r}_i(0) - \mathbf{r}_i(t)] \right\rangle, \quad (3)$$

where $G_S(r, t) d\mathbf{r}$ is proportional to the probability of finding a particle at distance \mathbf{r} after a time t if the same particle was in the origin $\mathbf{r} = \mathbf{0}$ at the initial time $t = 0$. The incoherent, or self, ISF can be written as

$$F_S(Q, t) = \left\langle \sum_{i=1}^N e^{i\mathbf{Q} \cdot [\mathbf{r}_i(t) - \mathbf{r}_i(0)]} \right\rangle. \quad (4)$$

In Fig. 4 we show the function $F_S(Q, t)$ for the different

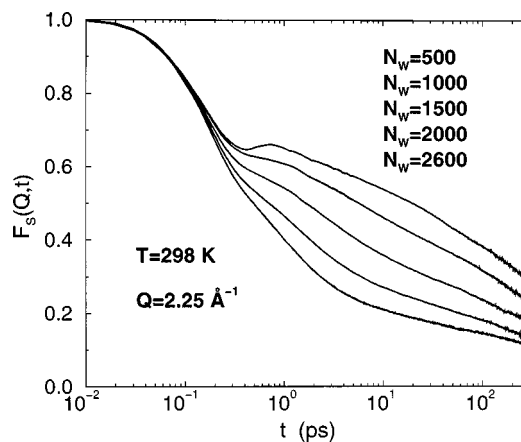


FIG. 4. Self intermediate scattering function (ISF) of the oxygen atoms at ambient temperature for $Q = 2.25 \text{ \AA}^{-1}$, the position of the maximum of the oxygen structure factor, for different levels of hydration from $N_w=500$ (top curve) to $N_w=2600$ (bottom curve). Q is averaged over all three dimensions.

hydrations calculated at the maximum of the oxygen–oxygen structure factor $Q_{\max}=2.25 \text{ \AA}^{-1}$, where the cage effect is expected to be strongest (see the discussion in Sec. II B). A shoulder appears in the correlators upon decreasing the hydration, and the long time relaxation behavior deviates strongly from the exponential form. It is evident that the interaction with the hydrophilic substrate plays a crucial role in the cage effect, since, at the lower levels of hydration, the fraction of molecules in contact with the surface is larger than at higher levels of hydration.

Apparently, lowering the hydration plays a role similar to supercooling the bulk liquid, but, in spite of some similarity with bulk supercooled water, here the late part of the ISFs cannot be fitted by the stretched exponential of Eq. (1), which is predicted by MCT.

Thus, at first glance our study of confined water appears to indicate that the water mobility is reduced relative to the bulk phase and that, as a function of hydration, a diversification of relaxation times develops analogous to supercooled systems undergoing a kinetic glass transition. Nonetheless, the deviation for the late part of the correlator from the analytical predictions of MCT has to be explained for a full understanding of the dynamics.

We must take into account in our analysis that the relaxation of the cage around the molecules close to the substrate is determined by the strong hydrophilic effect which leads to the formation of the double-layer structure of water close to the surface (see Fig. 2). The way in which the water molecules arrange themselves close to the substrate as well as the extension of the substrate perturbation affect the dynamical properties.

A more detailed examination of the contributions to the single-particle dynamics must therefore be performed by taking into account the possibility that the water molecules close to the Vycor surface could be much less mobile than the ones in the center of the pore, since the former ones are strongly H-bonded to the substrate.^{26,27}

For this reason we performed a layer analysis separating the contribution coming from the first two layers (the outer shells or outer layers) close to the substrate from the contribution coming from the remaining water in the inner shells (or inner layers).²⁹ The definition of these two subsets is inspired by the density profile (see Fig. 2). The outer shells are defined as $15 < R < 20 \text{ \AA}$ while the inner shells are the remaining $0 < R < 15 \text{ \AA}$.

In Fig. 5 we show the results of this analysis for the MSD at two different hydrations, roughly full hydration and half-hydration. Since the fluid is confined in the x and y directions we calculate separately the quantity along the z direction and along the radial (or xy) direction R . Both quantities are multiplied by the proper factor in order to adjust them to the three-dimensional scale for a direct comparison.

It is clearly seen that the diffusion of the molecules in the outer shells is much slower relative to the ones in the inner shells. We also observe that the change of hydration does not have a strong influence on the outer shells. We find that the diffusion is slower along xy but the shape of the MSD does not change relative to the one in the z direction. In fact, the outer water molecules do not reach the diffusive

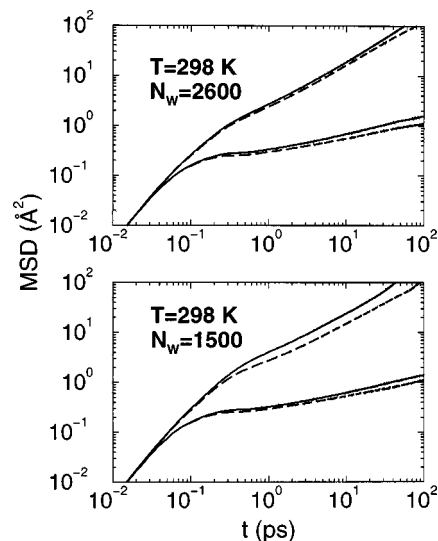


FIG. 5. Layer analysis of the MSD of the oxygen atoms at ambient temperature. The contributions of the water molecules in the inner layers (free water) and in the outer layers (bound water) are presented at ambient temperature for $N_w=2600$ (upper panel) and $N_w=1500$ (lower panel). The continuous lines represent diffusion along the z direction, while the dashed lines are for the diffusion along the xy direction.

regime during the observation time of Fig. 5 for both directions.

The results of the layer analysis for the ISF at full hydration are shown in Fig. 6 along the z direction (top) and along the xy direction (bottom). Water in the outer shells appears to be already in a glasslike state, since its ISF decays to zero over a much longer time scale. The behavior of the ISF from the inner layer contribution is different. We observe that the long time relaxation is characterized by a stretched exponential form, Eq. (1). The onset of the α relaxation is preceded by the fast relaxation, which is usually

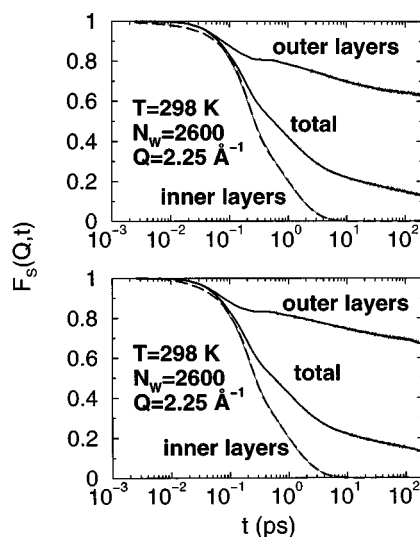


FIG. 6. Layer analysis of the self intermediate scattering function (ISF) at ambient temperature for $N_w=2600$ at the peak of the structure factor. The ISF is shown along the z direction (top) and along the xy direction (bottom). In both directions the contributions from free and bound water are shown separately in addition to the total ISF. The free water contribution is fitted by Eq. (5) (long dashed line).

TABLE III. Fit parameters of the lineshape, Eq. (5), to the ISF data at ambient temperature.

N_w	Direction	τ_l (ps)	β	τ_s (ps)
2600	xy	0.83	0.78	0.22
2600	z	0.84	0.79	0.21
1500	xy	1.4	0.67	0.19
1500	z	0.79	0.64	0.22

observed at short time both experimentally and in computer simulations of supercooled liquids. By taking into account the fast relaxation with an appropriate normalizing function in both directions, the entire curve can be described very well by two relaxation processes with different time scales,

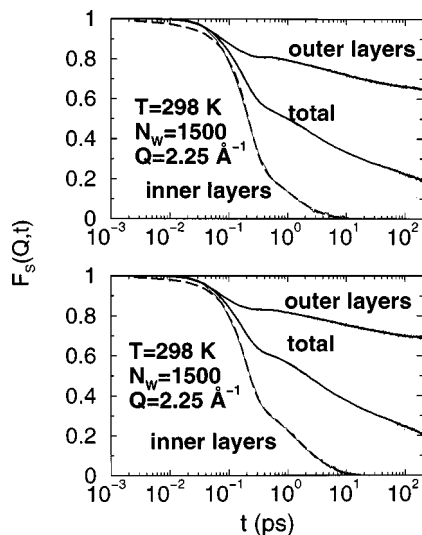
$$F_s(Q,t) = [1 - A(Q)]e^{-(t/\tau_s)^2} + A(Q)e^{-(t/\tau_l)^\beta}, \quad (5)$$

where the stretched exponential contains the long relaxation time τ_l and the Kohlrausch exponent β already introduced in Sec. II B. In this equation the normalizing function $A(Q)$ is the Debye–Waller factor, which is also termed the Lamb–Mössbauer factor for the single particle motion. $A(Q) = e^{-a^2 Q^2/3}$ accounts for the cage effect, with a the effective cage radius. The short time function is written in terms of an exponential containing the short relaxation time τ_s . The values extracted from the fit are reported in Table III.

In Fig. 7 the shell analysis for the ISF at $Q_{\max} = 2.25 \text{ \AA}^{-1}$ is shown at half-hydration, ($N_w = 1500$). The shell analysis works well also for this level of hydration, and the curves obtained from the inner layer contribution can be fitted by the functional form Eq. (5). The resulting parameters are also reported in Table III.

The τ parameters reported in Table III are similar to those of bulk water but β is much smaller⁵⁴ relative to the bulk where $\beta = 1$.⁴⁴ From the values of $A(Q)$ the cage radius can be extracted. We obtain $a \approx 0.5 \text{ \AA}$, again similar to the radius obtained for bulk water.

We note in passing that if only one layer is considered for the bound water, namely $17 < R < 20 \text{ \AA}$, then the fit to the

FIG. 7. Like Fig. 6 but for $N_w = 1500$.

stretched exponential of the remaining water is not completely satisfactory.⁵³ This confirms that the separation into the two subsets of water molecules chosen above is an appropriate representation of the two clearly distinct dynamical regimes coexisting in the liquid. It is unclear to what extent these effects would be visible in the experiments, where usually only the total ISF is measured. There are, however, experimental indications that two different subsets exist in H-bonded confined liquids.^{55,56}

We note that water shows an analogous behavior to what was found in mixtures, for example, with *n*-butoxyethanol. In this case dielectric relaxation studies show the existence of two kinds of water coexisting in the mixture: the hydration water and the ‘‘bulk’’ water.⁵⁷ Similar behavior has also been reported in a theoretical study of water in contact with a formic acid dimer, where significantly lower values of D have been observed in the first and second solvation region up to $\approx 4.5 \text{ \AA}$.⁵⁸ Moreover, the dynamics of a complex liquid, *o*-terphenyl (OTP), confined in nanometer scale pores can also be interpreted in terms of a two-layer model. Calorimetric measurements show, in fact, the existence of two glass transition temperatures for this latter system.²

Thermometric studies,^{59,60} NMR spectroscopy,^{59–62} neutron diffraction,^{59,63–66} and x-ray diffraction⁶⁷ can also be interpreted in terms of two types of water which are present in confining pores: *free water*, which is in the middle of the pore, and *bound water*, which resides close to the surface. Free water is observed to freeze abruptly in the cubic ice structure with a hysteresis in the melting/freezing transition which decreases at decreasing pore size. Bound water freezes gradually without any hysteresis effect, but it does not make any transition to an ice phase and it is called sometimes *nonfreezable water*.⁶⁷ Although all these experimental findings refer to static properties, we can reasonably identify the water molecules in the outer layers as *bound* and *not freezable* water while *free* water corresponds to the molecules in the inner layers of the simulated pore.

VI. CONFINED WATER AT SUPERCOOLED TEMPERATURES

For the discussion of supercooled confined water we consider the case close to half-hydration, $N_w = 1500$, which can be regarded as a reasonable compromise between computational effort and performing the layer analysis with sufficient statistical accuracy. As stated above, the temperature effect on the structure of the double layer of molecules close to the substrate is small (see Fig. 2). Therefore, the layer analysis is done using the same separation, $R = 15 \text{ \AA}$, as for the room temperature simulations.⁵⁴ The MSD along the z direction is shown for decreasing temperatures for the inner shells (free water) in Fig. 8 and the outer shells (bound water) in Fig. 9. The clear distinction between free and bound water at room temperature is maintained at all lower temperatures. It is clear from Fig. 8 that at lower temperatures the cage effect persists for longer times.

A. The ISF at Q_{\max} vs T

Figure 10 shows, as an example, the ISF for motion along the z direction at $T = 240 \text{ K}$ and $Q = Q_{\max} = 2.25 \text{ \AA}^{-1}$.

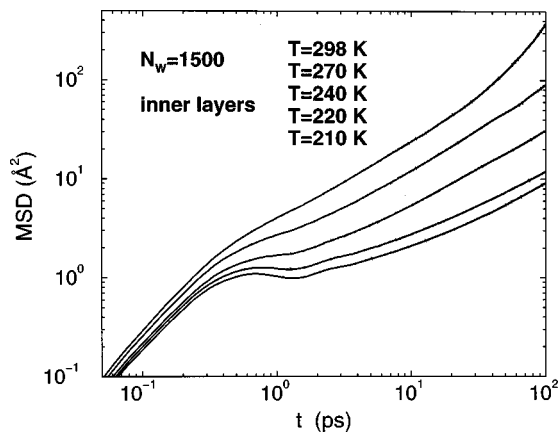


FIG. 8. MSD of free water at half-hydration along the z direction for five temperatures (298, 270, 240, 220, and 210 K, from top to bottom).

The inner layer contribution can be fitted very well by Eq. (5); we obtain $\beta=0.62$, $\tau_l=11$ ps, and $\tau_s=0.16$ ps. At this temperature a bump appears in the ISF of the free water at around 0.7 ps. Signatures of this feature are also visible in the MSD of Figs. 8 and 9 where oscillations in the plateau region are easily discernible. They are similar to features found in other simulation studies; for typically strong glass formers they can be attributed to the so-called Boson peak (BP).^{22,23,68,69}

We repeated the layer analysis of the ISF at Q_{\max} for all different temperatures studied. In Fig. 11 we show the results along the z direction for the inner layers as a function of temperature at $Q=Q_{\max}$. We wish to point out that there are no qualitative differences in the behavior along the xy direction, where, in particular, the same BP feature is present. We observe that, as the temperature is decreased, the shoulder of the slow relaxation becomes more and more pronounced.

The fit by Eq. (5) agrees very well in the whole range explored except for the region of the bump ascribed to the BP, which is not accounted for in the fitting function. Since we can carry out a precise line shape analysis by using only two relaxation processes, where the long time part is perfectly described by the α relaxation of the MCT, we can test

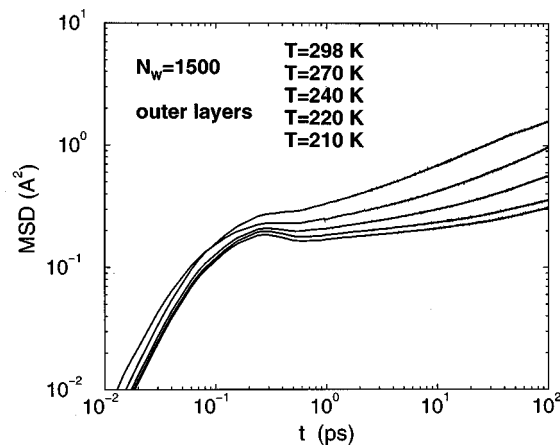


FIG. 9. MSD of bound water at half-hydration along the z direction for five temperatures (298, 270, 240, 220, and 210 K, from top to bottom).

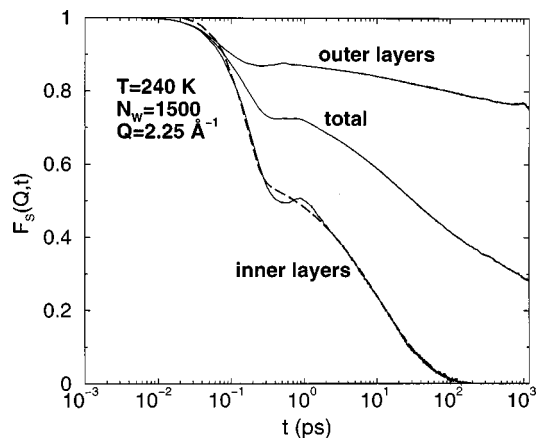


FIG. 10. Layer analysis of the ISF at $T=240$ K for $N_w=1500$ at $Q=2.25 \text{ \AA}^{-1}$ along the z direction. The contributions from the free (inner layers) and bound water (outer layers) are shown together with the total ISF. The free water curve is fitted by Eq. (5) (long dashed line). The bump in the free water ISF is evidence of the presence of a Boson peak.

the predictions of the MCT which concern the values for the Kohlrausch exponent β and the long relaxation time τ_l .

The values of τ_l and β obtained from the fits of the ISF at different temperatures are shown in Fig. 12 for both the xy and z directions. The validity of the asymptotic scaling law predicted by MCT implies that the stretching exponent β is temperature independent.⁴¹ For $T>T_C$ one expects $\beta(T \rightarrow T_C) \approx \beta_0 < 1$. In our case the exponent β approaches an asymptotic value around 0.5 in the xy direction and 0.6 along z as shown in the lower part of Fig. 12. A similar value is found for bulk water.

In the panels in the upper part we show that the relaxation time satisfies the MCT prediction Eq. (2). In the z direction (panel on the left) we estimate a temperature of structural arrest $T_C \approx 167.6$ K with an exponent $\gamma \approx 3.8$. Along the xy direction (panel on the right) the T_C is slightly higher $T_C \approx 170.4$ K with $\gamma \approx 3.4$.

This is in agreement with the idea that an enhancement of the free volume speeds up the dynamics leading to a de-

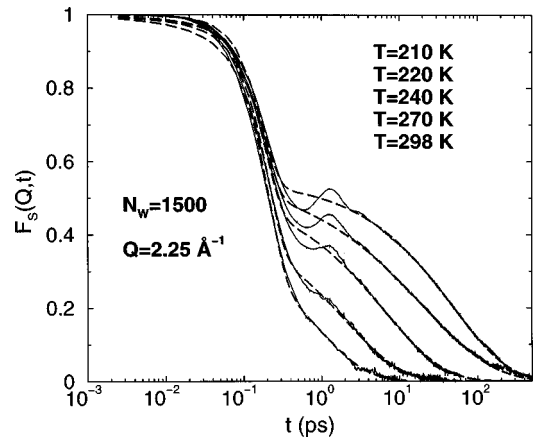


FIG. 11. The free water contribution to the ISF for $Q=2.25 \text{ \AA}^{-1}$ along the z direction at different temperatures, from $T=298$ K (bottom curve) to $T=210$ K (top curve). The curves are fitted by Eq. (5) (long dashed lines). It is evident that the bump, the region of which is excluded from the fit, increases with decreasing temperature.

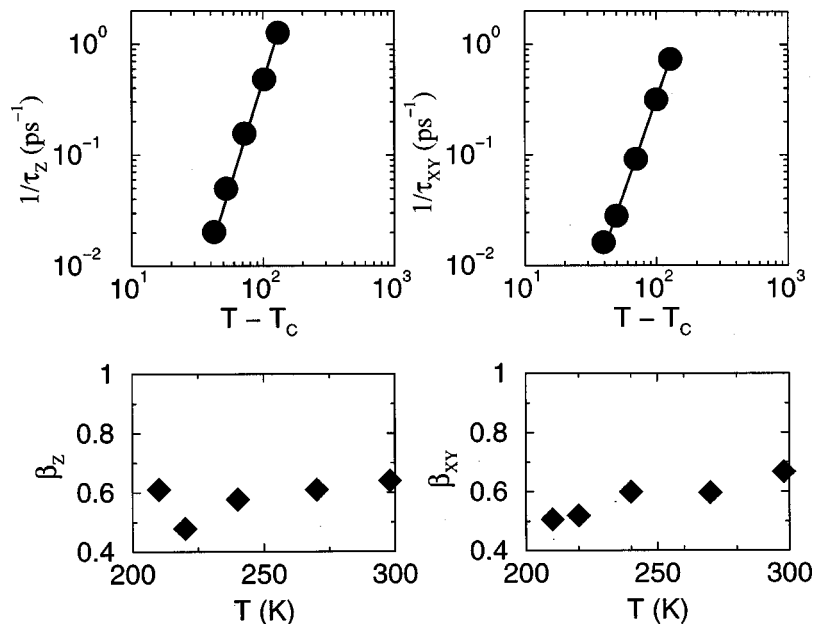


FIG. 12. Fit parameters. Top: log-log plots of the inverse relaxation time τ_i^{-1} as a function of $T - T_c$ along the z direction (left) and the xy direction (right). The full lines are power law fits given by $1/\tau_z \sim (T - 167.6)^{3.8}$ (left) and $1/\tau_{xy} \sim (T - 170.4)^{3.4}$ (right). Bottom: T dependence of the Kohlrausch exponents β along the z (left) and xy directions (right).

crease of the glass transition temperature relative to the bulk. At ambient pressure SPC/E bulk water undergoes a kinetic glass transition at $T = 186.3$ K with $\gamma = 2.29$.⁴⁴

B. The ISF at different Q

From the fits of the ISF at different wavelengths Q , shown for example along the z direction in Fig. 13 for $T = 240$ K, we obtain values of β and τ_i as a function of Q . Such values for the different temperatures are reported in Fig. 14 for the z direction and in Fig. 15 for the xy direction. The behavior of the parameters is compatible with the MCT.

As shown in the insets of both figures the Kohlrausch exponent β starts from values close to 1 at low Q and high temperatures and reaches a common plateau at large Q . This behavior is in agreement with the interpretation of the kinetic glass transition by MCT in terms of the cage effect, since for Q^{-1} larger than the cage size we expect to find that the stretching of the exponential at long time Eq. (1) is less relevant. Thus the Kohlrausch exponent is expected to go to 1 for large Q^{-1} when the system enters the normal Debye regime of diffusion in the long time decay region of the ISF. Of course this limit is reached at higher values of Q at higher temperatures, where the Debye regime is more easily established, as seen in the insets of Figs. 14 and 15. The oscillation in the plateau region does not allow for the calculation of the MCT parameters a and b related to the power laws of approach to and departure from the plateau. It is, however, shown that for large Q values the Kohlrausch exponent coincides with the scaling exponent b .⁷⁰ We therefore obtain $b \approx 0.4$ in this system for both the xy and the z directions.

τ_i^{-1} shows a linear behavior as a function of Q^2 in Figs. 14 and 15, where the continuous lines which have slope 1 are plotted as guidelines. This behavior is common for glass formers close to the kinetic glass transition and has been found, for instance, in glycerol.⁷¹ In the interpretation we must take into account that τ_i measures the time scale of the final relaxation of the cage with the subsequent decay of the

self-correlation function of the densities over the length scale Q^{-1} and the diffusion of the molecule over distances of the order Q^{-1} . In the diffusive regime valid for large Q^{-1} we expect $\tau_i^{-1} \sim Q^2$. At variance with bulk water we do not find any crossover of the behavior of τ_i^{-1} from a Q^2 to a Q proportionality at high Q ,⁴⁴ except, perhaps, at the lowest temperature.

In Fig. 13 there is a clear evidence of a bump at 0.7 ps which is preserved at the different temperatures as seen in Fig. 11 for $Q_{\max} = 2.25 \text{ \AA}^{-1}$. The position of the bump is independent of Q , which is clearly seen in Fig. 13 at $T = 240$ K and which is also found at all other explored temperatures. As mentioned in Sec. VI A, similar effects have been observed in computer simulations of other glass formers^{22,23,68,69} and have been attributed to the existence of a Boson peak (BP). The BP is present in many glasses as a

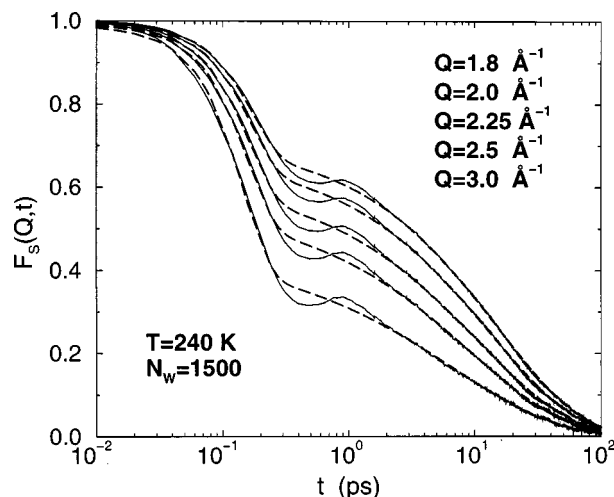


FIG. 13. The ISF along the z direction of the free water for half-hydration and $T = 240$ K for several values of Q from $Q = 1.8 \text{ \AA}^{-1}$ (top curve) to $Q = 3 \text{ \AA}^{-1}$ (bottom curve). All curves are fitted by Eq. (5) (long dashed lines), excluding the region around the bump.

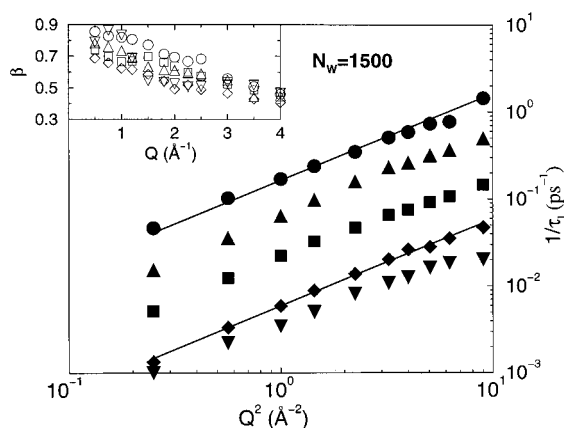


FIG. 14. Relaxation time τ_1 and exponent β (in the inset) of free water as extracted from the fits of the long time relaxation behavior of the ISF at different Q along the xy direction [Eq. (5)]. The continuous lines with slope 1 have been inserted as guidelines. Different symbols represent different temperatures; temperature decreases from top to bottom. Open symbols in the inset are for the same temperature as the corresponding full symbols in the figure.

consequence of an excess of vibrational modes and can be detected even in computer simulation in spite of the finite size effects.^{68,69} We do not want to enter into a detailed discussion of this behavior here, but we recall that the BP is considered as a precursor of a glass transition when it appears in the liquid state. We notice that as seen in Fig. 10, the BP feature appears clearly for the inner shells while it is much less evident in the outer layer contribution. While in some respect the substrate seems to enhance the effect relative to bulk water,⁴⁴ it appears that water in the outer shells is not able to sustain the vibrations which are considered responsible for the overshoot, possibly because we keep the atoms of the silica substrate rigid during the simulation. We intend to discuss this point more extensively in a future paper.

VII. COMPARISON WITH EXPERIMENTAL DATA

The technique that allows for the best comparison with our MD results is quasielastic neutron scattering (QENS). In

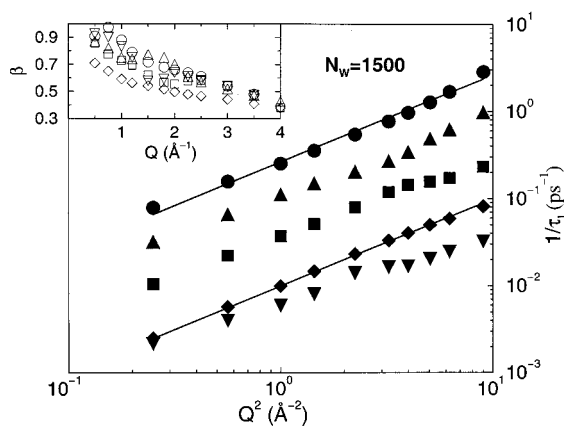


FIG. 15. Like Fig. 14, but along the z direction.

fact, the self-dynamic structure factor as measured by incoherent QENS is the time Fourier transform of the ISF. The first data that appeared in literature on water-in-Vycor were well fitted with a jump-diffusion model in a confined medium.⁷² This model was giving reasonable relaxation times, but the size of the confining region was unrealistic, 5 Å. An analysis based on MCT of those data was successively proposed.^{18,20} The data were also well fitted and the results were consistent with the appearance upon supercooling of a slow dynamics due to the approach to the kinetic glass transition. The Q dependence of the inverse of the structural relaxation time appeared for the 50% hydration level upon supercooling, as a power law with an exponent ranging from 2.51 to 2.06.²⁰ The fits however, were, performed on a limited Q range, approximately from 0.4 to 1.3 Å⁻¹. These findings have been confirmed by a recent QENS experiment where a full set of high-resolution data on water confined in Vycor glass has been analyzed for different hydration levels upon supercooling.²¹ The experimental exponents obtained from the fits to a limited range of Q appear to be slightly different from ours. In fact we find (see Figs. 14 and 15) a value which is approximately 2 at high temperatures and slightly decreases for the lowest temperature. However, an analysis performed on a more extended Q value data, up to 1.8 Å⁻¹, showed an exponent which is 2 at high temperature and decreases at lower temperatures, similar to what we found in the present simulation.⁷³

It is important to notice that the QENS response function is able to probe only the mobile water, namely the water above T_C , because of experimental resolution limitations. Therefore the experimental data appear so far compatible with our findings.

VIII. SUMMARY AND CONCLUSIONS

In this article we presented the results obtained by molecular dynamics on the single particle dynamics of SPC/E water confined in a silica pore, which represents an approximation to the system of water confined in Vycor. This system can also be considered as representative of the more general case of water confined in a hydrophilic nanopore.

Through the study of dynamic time correlators such as the mean square displacement (MSD) and the self part of the intermediate scattering factor (ISF), we investigated the onset of slow dynamics when the hydration level in the pore is decreased or when the liquid is supercooled.

At ambient temperature we found that upon decreasing the hydration level a flattening of the MSD takes place after the initial ballistic regime and before the onset of the stochastic diffusion. In correspondence a two-step relaxation behavior appears in the ISF, which displays a strongly non-exponential decay at long time. In this way the single-particle dynamics has the signatures of the presence of a cage effect as predicted by mode coupling theory (MCT).

Apparently the effect of hydration is similar to the effect of supercooling in bulk water, but the long time relaxation of the ISF cannot be fitted by the stretched exponential predicted by the MCT. By performing a layer analysis it becomes possible to separate the contribution to the dynamics of the water molecules close to the substrate (bound water)

from the contribution coming from the molecules which are in the internal layers (free water). The subset of molecules belonging to the bound water shows density oscillations and appears to be in a glassy state with very low mobility already at ambient conditions. The free water shows a dynamical behavior typical of glass forming liquids. This behavior can be accounted for by the idealized MCT in analogy with previous findings on SPC/E water in the bulk phase.^{44,46,47} We would like to stress, however, that in the present work we have considered a much more complex system than the bulk, where an additional anisotropic effect and a perturbation by the substrate is present.

The fact that MCT could be used in this framework as a unifying theoretical approach is highly relevant as a guideline for the systematic study of the important phenomenology of confined and interfacial water.

We show evidence that the hydration level together with the hydrophilicity of the substrate play, through the layering effect, an important role in determining the dynamical properties of confined water. As far as the anisotropy of the system is concerned, we did not observe large differences in the behavior along the confined direction (xy) and along the pore axis (z), where periodic boundary conditions are applied, apart from the fact that the mobility along the xy direction is smaller than in the z direction.

By supercooling confined water at half-hydration we have found that the subset of free water undergoes a kinetic glass transition, which can be described in terms of the MCT. The layer analysis makes possible the calculation of various important quantities related to the glass transition, like the temperature of structural arrest, T_C , and the critical exponent, γ . Similar results have been obtained from a preliminary analysis of the full hydration case.⁷⁴

MCT has been largely used in the interpretation of the phenomenology of liquids in the supercooled phase. In the recent attempts to develop a unified first-principles theory for the glass transition it has been recognized that MCT keeps its validity in describing the liquid just above the temperature T_C . It is time to test this theory for confined fluids, where, in spite of the experimental and computer simulation efforts, the phenomenology of the dynamics of the confined and interfacial liquids upon supercooling is still unclear. We have shown evidence that the MCT can be applied to the interpretation of the dynamical behavior of supercooled confined water, if the layering effects determined by the interaction with the hydrophilic substrate are carefully taken into account. We believe that the results obtained in this work are of great importance in understanding the phenomenology of the mobility of fluids in nanopores.

ACKNOWLEDGMENTS

P. G. and M. R. are indebted to M. A. Ricci for her contribution to the early stages of this work. P. G. furthermore thanks Barbara Coluzzi, Daniele Fioretto, Mattias Fuchs, Jorge Kohanoff, Friedrich Kremer, Ruth M. Lynden-Bell, Gregory B. McKenna, and Ajay P. Singh for helpful conversations. We additionally thank Barbara Coluzzi and

Francesco Sciortino for a critical reading of the manuscript. The financial support of the G Section of INFM is gratefully acknowledged.

- ¹ See, for example, the Proceedings of the International Workshop on "Dynamics in Confinement," edited by B. Frick, R. Zorn, and H. Büttner, *J. Phys. IV* **10** (2000).
- ² J.-Y. Park and G. B. McKenna, *Phys. Rev. B* **61**, 6667 (2000).
- ³ A. Huwe, F. Kremer, P. Behrens, and W. Schwieger, *Phys. Rev. Lett.* **82**, 2338 (1999).
- ⁴ M. Arndt, R. Stannarius, H. Groothues, E. Hempel, and F. Kremer, *Phys. Rev. Lett.* **79**, 2077 (1997).
- ⁵ Z. T. Németh and H. Löwen, *Phys. Rev. E* **59**, 6824 (1999) and references therein.
- ⁶ M. S. P. Sansom, I. K. Kerr, J. Breed, and R. Sankaramakrishnan, *Biophys. J.* **70**, 693 (1996).
- ⁷ R. M. Lynden-Bell and J. C. Rasaiah, *J. Chem. Phys.* **105**, 9266 (1996) and references therein.
- ⁸ M. Settles and W. Doster, *Faraday Discuss.* **103**, 269 (1996).
- ⁹ H. E. Stanley, *MRS Bull.* **24**(5), 22 (1999).
- ¹⁰ C. A. Angell, *Annu. Rev. Phys. Chem.* **34**, 593 (1983).
- ¹¹ For a review on metastable liquids and water in particular, see P. G. Debenedetti, *Metastable Liquids: Concepts and Principles* (Princeton U.P., Princeton, NJ, 1997).
- ¹² T. Fehr and H. Löwen, *Phys. Rev. E* **52**, 4016 (1995).
- ¹³ B. Böttcher and H. Teichler, *Phys. Rev. E* **59**, 1948 (1999).
- ¹⁴ P. Scheidler, W. Kob, and K. Binder, *J. Phys. IV* **10**, Pr7-33 (2000); P. Scheidler, W. Kob, and K. Binder, preprint cond-mat/0003257.
- ¹⁵ See, e.g., I. Brovchenko, D. Paschek, and A. Geiger, *J. Chem. Phys.* **113**, 5026 (2000); A. Kohlmeyer, C. Hartnig, and E. Spohr, *J. Mol. Liq.* **78**, 233 (1998); J. C. Shelley, G. N. Patey, D. R. Berard, and G. M. Torrie, *J. Chem. Phys.* **107**, 2122 (1997); S. B. Zhu and G. W. Robinson, *ibid.* **94**, 1403 (1991); E. Spohr, *J. Phys. Chem.* **93**, 6171 (1989); many more references can be found in these publications or in E. Spohr, "Computer Simulations of Electrochemical Interfaces," in *Advances in Electrochemical Science and Engineering*, edited by R. C. Alkire and D. M. Kolb (Wiley-VCH, Weinheim, 1999), Vol. 6, p. 1.
- ¹⁶ R. Radhakrishnan, K. E. Gubbins, and M. Sliwinska-Bartkowiak, *J. Chem. Phys.* **112**, 11048 (2000).
- ¹⁷ S. H. Chen and M. C. Bellissent-Funel, in *Hydrogen Bond Networks*, edited by M. C. Bellissent-Funel and J. C. Dore, NATO ASI Series C: Mathematical and Physical Science (Kluwer Academic, Dordrecht, 1994), Vol. 435, p. 337.
- ¹⁸ S.-H. Chen, P. Gallo, and M. C. Bellissent-Funel, *Can. J. Phys.* **73**, 703 (1995).
- ¹⁹ V. P. Denisov and B. Halle, *Faraday Discuss.* **103**, 227 (1996).
- ²⁰ S.-H. Chen, P. Gallo, and M. C. Bellissent-Funel, in *Non-Equilibrium Phenomena in Supercooled Fluids, Glasses and Amorphous Materials*, edited by M. Giordano, D. L. Leporini, and M. P. Tosi (World Scientific, Singapore, 1996), p. 186.
- ²¹ J.-M. Zanotti, M.-C. Bellissent-Funel, and S.-H. Chen, *Phys. Rev. E* **59**, 3084 (1999).
- ²² A. Paciaroni, A. R. Bizzarri, and S. Cannistraro, *Phys. Rev. E* **60**, R2476 (1999).
- ²³ A. Paciaroni, A. R. Bizzarri, and S. Cannistraro, *Phys. Rev. E* **57**, R6277 (1999).
- ²⁴ F. Bruni, M. A. Ricci, and A. K. Soper, *J. Chem. Phys.* **109**, 1478 (1998).
- ²⁵ A. K. Soper, F. Bruni, and M. A. Ricci, *J. Chem. Phys.* **109**, 1486 (1998).
- ²⁶ E. Spohr, C. Hartnig, P. Gallo, and M. Rovere, *J. Mol. Liq.* **80**, 165 (1999).
- ²⁷ C. Hartnig, W. Witschel, E. Spohr, P. Gallo, M. A. Ricci, and M. Rovere, *J. Mol. Liq.* **85**, 127 (2000).
- ²⁸ W. Götze and L. Sjögren, *Rep. Prog. Phys.* **55**, 241 (1992); W. G. Götze, in *Liquids, Freezing and Glass Transition*, Les Houches Session LI, 1989, edited by J. P. Hansen, D. Levesque, and J. Zinn-Justin (North Holland, Amsterdam 1991).
- ²⁹ P. Gallo, M. A. Ricci, M. Rovere, C. Hartnig, and E. Spohr, *Europhys. Lett.* **49**, 183 (2000).
- ³⁰ M. Mezard and G. Parisi, *J. Chem. Phys.* **111**, 1076 (1999).
- ³¹ M. Mezard and G. Parisi, *Proceedings of the ICTP Trieste Workshop on "Unifying Concepts in Glass Physics,"* Trieste, 15–18 September 1999, edited by S. Franz, S. C. Glotzer, and S. Sastry [*J. Phys.: Condens. Matter* **12**, 6295 (2000)]; M. Mezard, *Physica A* **265**, 352 (1999).

- ³²A. W. Kauzmann, *Chem. Rev.* **43**, 219 (1948).
- ³³J. H. Gibbs and E. A. Di Marzio, *J. Chem. Phys.* **28**, 373 (1958); G. Adam and J. H. Gibbs, *ibid.* **43**, 139 (1965).
- ³⁴F. H. Stillinger and T. A. Weber, *Phys. Rev. A* **25**, 978 (1982); F. H. Stillinger, *Science* **267**, 1935 (1995).
- ³⁵S. Sastry, P. G. Debenedetti, and F. H. Stillinger, *Nature (London)* **393**, 554 (1998).
- ³⁶A. Cavagna, I. Giardina, and G. Parisi, *Phys. Rev. B* **57**, 11251 (1998).
- ³⁷E. La Nave, A. Scala, F. W. Starr, F. Sciortino, and H. E. Stanley, *Phys. Rev. Lett.* **84**, 4605 (2000).
- ³⁸C. Donati, F. Sciortino, and P. Tartaglia, *Phys. Rev. Lett.* **85**, 1464 (2000).
- ³⁹B. Coluzzi, M. Mezard, G. Parisi, and P. Verrocchio, *J. Chem. Phys.* **111**, 9039 (1999); B. Coluzzi, G. Parisi, and P. Verrocchio, *ibid.* **112**, 2933 (2000).
- ⁴⁰F. Sciortino, W. Kob, and P. Tartaglia, *Phys. Rev. Lett.* **83**, 3214 (1999).
- ⁴¹W. Götze, *J. Phys.: Condens. Matter* **11**, A1 (1999).
- ⁴²W. Götze and L. Sjögren, *Z. Phys. B: Condens. Matter* **65**, 415 (1987).
- ⁴³H. J. C. Berendsen, J. R. Grigera, and T. P. Straatsma, *J. Phys. Chem.* **91**, 6269 (1987).
- ⁴⁴P. Gallo, F. Sciortino, P. Tartaglia, and S.-H. Chen, *Phys. Rev. Lett.* **76**, 2730 (1996); F. Sciortino, P. Gallo, P. Tartaglia, and S.-H. Chen, *Phys. Rev. E* **54**, 6331 (1996).
- ⁴⁵R. J. Speedy and C. A. Angell, *J. Chem. Phys.* **65**, 851 (1976).
- ⁴⁶W. Starr, F. Sciortino, and H. E. Stanley, *Phys. Rev. E* **60**, 6757 (1999).
- ⁴⁷L. Fabbian, A. Latz, R. Schilling, F. Sciortino, P. Tartaglia, and C. Theis, *Phys. Rev. E* **60**, 5768 (1999).
- ⁴⁸Y. Hirama, T. Takahashi, M. Hino, and T. Sato, *J. Colloid Interface Sci.* **184**, 349 (1996).
- ⁴⁹P. H. Poole, F. Sciortino, U. Essmann, and H. E. Stanley, *Nature (London)* **360**, 324 (1992); *Phys. Rev. E* **48**, 3799 (1993).
- ⁵⁰L. A. Baets and P. Clancy, *J. Chem. Phys.* **101**, 9837 (1994).
- ⁵¹A. Brodka and T. W. Zerda, *J. Chem. Phys.* **104**, 6319 (1996).
- ⁵²M. J. Benham, J. C. Cook, J. C. Li, D. K. Ross, P. L. Hall, and B. Sarkissian, *Phys. Rev. B* **39**, 633 (1989).
- ⁵³P. Gallo, M. Rovere, M. A. Ricci, C. Hartnig, and E. Spohr, *Philos. Mag. B* **79**, 1923 (1999).
- ⁵⁴P. Gallo, *Phys. Chem. Chem. Phys.* **2**, 1607 (2000).
- ⁵⁵Y. B. Mel'nichenko, J. Schüller, R. Richert, B. Ewen, and C. K. Loong, *J. Chem. Phys.* **103**, 2016 (1995).
- ⁵⁶V. Crupi, D. Majolino, P. Migliardo, and V. Venuti, *J. Phys. Chem.* (in press).
- ⁵⁷D. Fioretto, A. Marini, G. Onori, L. Palmieri, A. Santucci, G. Socino, and L. Verdini, *Chem. Phys. Lett.* **196**, 583 (1992); D. Fioretto, A. Marini, M. Massarotti, G. Onori, L. Palmieri, A. Santucci, and G. Socino, *J. Chem. Phys.* **99**, 8115 (1993).
- ⁵⁸J. Kohanoff, S. Koval, D. A. Estrin, D. Laria, and Y. Abashkin, *J. Chem. Phys.* **112**, 9498 (2000).
- ⁵⁹T. Takamuku, M. Yamagami, H. Wakita, Y. Masuda, and T. Yamaguchi, *J. Phys. Chem. B* **101**, 5730 (1997).
- ⁶⁰E. W. Hansen, H. C. Gran, and E. J. Sellevold, *J. Phys. Chem. B* **101**, 7027 (1997).
- ⁶¹S. Stapf and R. Kimmich, *J. Chem. Phys.* **103**, 2247 (1995).
- ⁶²E. W. Hansen, E. Tangsted, E. Myrvold, and T. Myrstad, *J. Phys. Chem. B* **101**, 10709 (1997).
- ⁶³D. C. Steytler, J. C. Dore, and C. J. Wright, *J. Phys. Chem.* **87**, 2458 (1983).
- ⁶⁴D. C. Steytler and J. C. Dore, *Mol. Phys.* **56**, 1001 (1985).
- ⁶⁵J. C. Dore, M. Dunn, and P. Chieux, *J. Phys.* **48**, C1 (1987).
- ⁶⁶M. C. Bellissent-Funel, J. Lal, and L. Bosio, *J. Chem. Phys.* **98**, 4246 (1993).
- ⁶⁷K. Morishige and K. Kawano, *J. Chem. Phys.* **110**, 4867 (1999).
- ⁶⁸J. Horbach, W. Kob, K. Binder, and C. A. Angell, *Phys. Rev. E* **54**, R5897 (1996).
- ⁶⁹J. Horbach, W. Kob, and K. Binder in *Neutrons and Numerical Methods*; edited by M. R. Johnson, G. J. Kearley, and H. G. Buttner (AIP, Woodbury, 1999), p. 136.
- ⁷⁰M. Fuchs, *J. Non-Cryst. Solids* **172–174**, 241 (1994).
- ⁷¹W. Petry and J. Wuttke, *Transp. Theory Stat. Phys.* **24**, 1075 (1995).
- ⁷²M.-C. Bellissent-Funel, S.-H. Chen, and J.-M. Zanotti, *Phys. Rev. E* **51**, 4558 (1995).
- ⁷³F. Bruni, S.-H. Chen, A. Deriu, P. Gallo, and M. A. Ricci, in preparation.
- ⁷⁴P. Gallo, M. Rovere, and E. Spohr, *Phys. Rev. Lett.* **85**, 4317 (2000).